Drift wave turbulence and zonal flow development measured by information rate

OPEN ACCESS
IOP Publishing
Plasma Physics and Controlled Fusion
Plasma Phys. Control. Fusion **67** (2025) 035021 (13pp)
https://doi.org/10.1088/1361-6587/adb5b5

Drift wave turbulence and zonal flow development measured by information rate

B Hnat[1,*], P Fuller[1,2], E Kim[2,3,4] and R Hollerbach[5]

[1] Physics Department, University of Warwick, Coventry CV4 7AL, United Kingdom
[2] Fluid and Complex Systems Research Centre, Coventry University, Coventry CV1 2TT, United Kingdom
[3] Nuclear Research Institute for Future Technology and Policy, Seoul National University, Seoul 08826, Republic of Korea
[4] Isaac Newton Institute for Mathematical Sciences, Cambridge CB3 0EH, United Kingdom
[5] Department of Applied Mathematics, University of Leeds, Leeds LS2 9JT, United Kingdom

E-mail: b.hnat@warwick.ac.uk

Received 2 September 2024, revised 17 January 2025
Accepted for publication 13 February 2025
Published 21 February 2025

Abstract

Generation of zonal flows (ZF) by drift wave turbulence in numerical simulations based on the modified Hasegawa–Wakatani model is investigated using probability density functions (PDFs) and information rate which quantifies the number of statistically distinct states generated per unit time in the non-equilibrium system. The evolution of time-dependent PDFs of the electrostatic potential, density, and vorticity is quantified by the information rate and is directly compared. We examine this evolution for the system dominated by the isotropic turbulence as well as the system dominated by anisotropic ZF. Impact of ZF on turbulence is captured by a narrower PDF of fluctuating velocity perpendicular to ZF. The information rates of the turbulent potential and density, which are coupled via fast electron parallel transport, are similar confirming the strong coupling between these quantities during their evolution. In contrast, zonal parts of these fields exhibit a distinct information rate evolution. This suggests that the zonal density structure may develop independently of ZF, consistent with recent finding in gyrokinetic simulations.

Keywords: drift wave turbulence, zonal flows, information rate

1. Introduction

The first generation of magnetic confinement fusion reactors will probably operate under enhanced confinement mode, to maintain a reasonable reactor size. The high confinement mode (H-mode) [1] is the most promising operating scenario currently considered for ITER [2] and STEP [3]. It is well-known that the transition from the low-confinement L-mode to the high-confinement H-mode, referred to as the L–H transition, requires external power input near or at the empirical threshold, which has non-trivial dependence on the mean density [4] and on plasma composition [5]. While the H-mode has been practically accessed in all tokamaks, including spherical ones, the physical mechanisms that control plasma transition from L-mode to H-mode are still debated [6–8].

The most popular paradigm for the L–H transition relies on the suppression of turbulent radial transport of energy and plasma [9, 10] by strongly sheared large-scale poloidal flows

* Author to whom any correspondence should be addressed.

[11–13]. Turbulent velocity fluctuations drive poloidal *zonal flows* (ZF) via the Reynolds stress action [14, 15]. In the slab geometry, zonal flows have radial length-scale comparable to the largest turbulent structures, and their length-scale in the poloidal direction is comparable to the system size [16]. The radial jet pattern is quasi-stationary, that is, it has no radial group velocity and the poloidal wave number $k_\theta = 0$. In the toroidal geometry, however, these flows may develop finite poloidal wave number through coupling to poloidally asymmetric density fluctuations and low wave number side bands [16, 17] and are distinct from the residual poloidal flows, called zero frequency ZF (ZFZF) or mean flows [18]. Zero-dimensional prey-predator models which include nonlinear interaction of ZFZF with turbulence and ZF shear [14, 19–22] demonstrated that both flows are important for the L–H transition. A direct causal link between the development of the strong shear and the L–H transition is difficult to establish experimentally. Most experimental results measure correlations between the depth of radial electric field well and turbulence levels [23–25] or the magnitude of the mean flow and the power threshold required to reach the H-mode [5].

The modified Hasegawa–Wakatani (MHW) equations [26–28] provide the simplest self-consistent model which exhibits turbulent fluctuations with anisotropic energy transfer from turbulence to large-scale flows. The resistive drift wave instability drives turbulent fluctuations in the presence of the fixed density gradient. Fast parallel electron response along the magnetic field maintains quasi-neutrality against polarisation drift-induced charge separation. This system of equations has been extensively studied numerically in the past [29–32].

The main aim of this paper is to present a novel statistical analysis using time-dependent probability density functions (PDFs) and the information theory to analyse simulation data from this model. In particular, the information rate detailed in § 2.2 quantifies the number of distinct statistical states generated by the system during its evolution in time (see [33, 34] for review), and is more suited to the analysis of systems far from equilibrium such as magnetically confined plasma. The remainder of this paper is organised as follows. Section 2 introduces our model and information rate. The key results are presented and discussed in § 3 including the snapshots of profiles, time-dependent PDFs and information rates. Section 4 contains Discussion and Conclusions.

2. Methodology

2.1. Hasegawa–Wakatani model

The MHW model captures the key features observed experimentally at the edge of the MCF plasma. These include resistive drift instability, onset of drift turbulence and the self-organisation of plasma into ZF [35].

The MHW equations describe the dynamics of the plasma density n and the electrostatic potential ϕ, with a fixed background density gradient and in the presence of parallel electron resistivity. The model is valid for cold ions, $T_i/T_e \ll 1$, and at low frequencies $\omega \ll \omega_{ci}$, where ω_{ci} is the ion gyrofrequency. Fields n and ϕ can be decomposed into their turbulent fluctuations, $\tilde{n}$, $\tilde{\phi}$, and zonal averages $\langle n \rangle$ and $\langle \phi \rangle$, such that $n = \tilde{n} + \langle n \rangle$ and $\phi = \tilde{\phi} + \langle \phi \rangle$. The angular brackets $\langle \dots \rangle$ correspond to poloidal averages which in the slab geometry are equivalent to integration along the poloidal line at a given radial location:

$$\langle f \rangle = \frac{1}{L_y} \int_0^{L_y} f \mathrm{d}y. \tag{1}$$

The MHW equations are then given by:

$$\frac{\partial n}{\partial t} = -\kappa \frac{\partial \phi}{\partial y} + A' \left(\tilde{\phi} - \tilde{n} \right) + [n, \phi] + D \nabla^2 n, \tag{2}$$

$$\frac{\partial}{\partial t} \nabla^2 \phi = A' \left(\tilde{\phi} - \tilde{n} \right) + \left[\nabla^2 \phi, \phi \right] + \mu \nabla^2 \left(\nabla^2 \phi \right), \tag{3}$$

where the density n and the potential ϕ are normalized, $n/n_0 \to n$ and $e\phi/T_e \to \phi$. The key parameters are defined as follows: $\kappa = \rho_s / L_n$, where the characteristic length-scale of the fixed background density gradient is given by $L_n = n_0/|\nabla n_0|$, and $\rho_s = \sqrt{m_i T_e}/eB$ is the hybrid Larmor radius. Time t and spatial coordinates x, y are normalised so that $\omega_{ci} t \to t$ and $\rho_s(x, y) \to (x, y)$. The coordinate system is defined so that x and y are aligned with the radial and poloidal directions, respectively, and the magnetic field is in the z direction.

Poisson brackets have their usual meaning, $[a, b] = (\partial a/\partial x)(\partial b/\partial y) - (\partial a/\partial y)(\partial b/\partial x)$. The dissipation coefficient D is the cross-field ambipolar diffusion coefficient, and μ is the ion perpendicular viscosity. The parameter A' controls the strength of the resistive coupling between n and ϕ:

$$A' = \frac{T_e k_{||}^2}{n_0 e^2 \eta \omega_{ci}}, \tag{4}$$

where η is electron resistivity and $k_{||}$ is the wave number in the direction of the magnetic field. This adiabatic parameter $A = A'/\kappa$ determines the degree to which electrons can move along the magnetic field to establish a perturbed Boltzmann density response. Importantly, the MHW equations exhibit a sharp bifurcation in their final quasi-stationary state, from isotropic vortex-like turbulent fluctuations for $A \lesssim 0.1$ to anisotropic ZF dominated state for $A \gtrsim 0.3$. The exact value of A for which this bifurcation occurs depends on the values of the dissipative terms used in the numerical simulation. In general, when $A \to \infty$ the density fluctuations become controlled by the potential fluctuations and MHW becomes identical to a Charney–Hasegawa–Mima equation [36]. The opposite limit $A \to 0$ is equivalent to the incompressible two-dimensional Euler equation. A finite non-zero A yields an unstable growth of drift waves providing a forcing mechanism that stops the vorticity from decaying to zero, as observed for the unforced Navier–Stokes equation. There are stable and unstable waves, as well as non-modal solutions of the system.

Applying flux-surface averaging (1) to equations (2) and (3) one obtains evolution equations for zonal component of zonal

density $\langle n\rangle$ and zonal vorticity $\langle\omega\rangle = \nabla^2\langle\phi\rangle$ as:

$$\frac{\partial\langle n\rangle}{\partial t} = \frac{\partial}{\partial x}\langle n\frac{\partial\phi}{\partial y}\rangle + D\nabla^2\langle n\rangle, \tag{5}$$

$$\frac{\partial\langle\omega\rangle}{\partial t} = \frac{\partial}{\partial x}\langle\omega\frac{\partial\phi}{\partial y}\rangle + \mu\nabla^2\langle\omega\rangle. \tag{6}$$

Stationary solutions of these equations are given by the balance between divergence of the radial flux of the relevant quantity and its dissipation. In the ideal case the potential vorticity $\Pi = \omega - n + \kappa x$ is the constant of motion for equations (2) and (3). This is reduced to $\langle\Pi\rangle = \langle\omega\rangle - \langle n\rangle$ for zonal averages.

We solve equations (2) and (3) numerically on a square grid of size $L=40$ (that is, $40\rho_s$ in dimensional units) with 1024 grid points in each of the x and y directions, and with periodic boundary conditions. The final stage of the MHW evolution is dominated by ZF due to lack of poloidal damping which is present in real laboratory plasmas and in 3D simulations. We compute the information rate of the density n, potential ϕ and the vorticity $\omega = \nabla^2\phi$. We explore all stages of the system's evolution, from the initial growth of the drift waves through the vortex-dominated turbulent state, and to the final ZF-dominated state. Three simulations with different adiabatic parameter $A = 0.01, 0.1, 1.0$ are studied. Increasing value of the parameter A corresponds to a higher contribution from the volume-averaged zonal fluctuations energy to the total energy of the system in the final stage of the system's evolution. Hence, the final quasi-stationary state of the system is dominated by the isotropic turbulence for $A = 0.01$, while anisotropic ZF state dominates the final state of the system with $A = 1.0$. The simulation with $A = 0.1$ represents the intermediate state.

In all cases dissipation coefficients $D = \mu = 0.01$, and the normalised background density gradient $\kappa = 1$. The initial condition was randomly generated values of the potential and density between 0 and 10^{-3}. The time step $\mathrm{d}t = 0.001$ is a compromise between well-resolved dynamics and the ability to perform long runs for a given parameter A. In all cases the simulation was run to a quasi-stationary state, in which the total energy did not change more than 1% over 100 time units.

2.2. Information Rate

Consider a stochastic variable x, which represents the evolution of a system far from equilibrium. A key characteristic of such a system is the dependence of the PDF of x on time, $p(x,t)$. Measuring the relative change between two adjacent PDFs $p(x,t)$ and $p(x,t+\delta t)$ in the limit as $\delta t \to 0$, we can define the information rate Γ as (see [33, 34] for review)

$$\Gamma^2(t) = \int_{-\infty}^{\infty}\frac{1}{p(x,t)}\left[\frac{\partial p(x,t)}{\partial t}\right]^2 \mathrm{d}x = 4\int_{-\infty}^{\infty}\left[\frac{\partial q(x,t)}{\partial t}\right]^2 \mathrm{d}x. \tag{7}$$

Here, $q(x,t) = \sqrt{p(x,t)}$. We use the second expression (in terms of q) in equation (7) to avoid difficulties when $p \approx 0$ in the denominator of the first expression. This is not a singularity, due to the $(\partial_t p)^2$ in the numerator, but it can cause difficulties when dividing a numerically estimated $(\partial_t p)^2$ by extremely small numbers.

There are several advantages in using the information rate over other statistical measures for systems far from equilibrium. For instance, unlike entropy which quantifies the width of a PDF, the information rate is sensitive to changes in time in the mean of the stochastic variable x or in PDF tails associated with rare, large events. The measure is also invariant under any time-independent change of variable. Unlike approaches based on moments of the PDF, which weight the PDF contribution by the power of a fluctuation, the information rate samples the entire PDF uniformly and thus gives a better representation of the evolution of an individual quantity in time. The information rate gives a characteristic time-scale over which the statistical state of a given variable is significantly changed. This gives physical insight into the system's dynamics that may not be achieved via the mean field approach.

The utility of information rate in capturing correlation and self-organisation, and forecasting bursts was demonstrated in dynamical systems [33, 34, 37] as well as L–H transitions [20–22, 38], working better than other statistical measures (e.g. kurtosis, skewness) or entropy-based information measures. It was also applied to the analysis of simulation results of the Hasegawa–Wakatani model [39] as well as a global circulation model [40].

3. Results

In this section, we provide key results in terms of profiles, PDFs and information rates of the electrostatic potential ϕ, density n and vorticity ω.

3.1. Profiles

Figures 1–3 show snapshots of potential ϕ (top row), density n (middle row) and vorticity (bottom row) for simulations with the adiabatic parameter $A = 0.01$, $A = 0.1$ and $A = 1.0$, respectively. We show these at five selected times, which represent distinct phases of the system evolution: drift wave growth, transition to isotropic turbulence, growth in the amplitude of turbulent fluctuations, development of ZF and the approximately time-stationary final state. These stages are reached at different times depending on the value of the parameter A. In figure 1, isotropic turbulence stage is reached at $t \approx 120$ and the anisotropic ZF is absent even at the final time $t = 250$. This is a known feature of the MHW model, which undergoes the bifurcation from ZF dominated dynamics to isotropic turbulence as the parameter A is decreased [29]. For $A = 0.1$ and $A = 1.0$ ZF dominate at the end of the simulation. Focusing on the simulation with $A = 0.1$ we observe that times $t = 10 - 40$ show the onset and the growth of the drift waves with poloidal wave number $k_\theta \approx 1\rho_s^{-1}$. At time $t = 60$ the system is in its turbulent state, dominated by vortex-like structures. At times $t = 120$ and $t = 250$ the electrostatic potential is already dominated

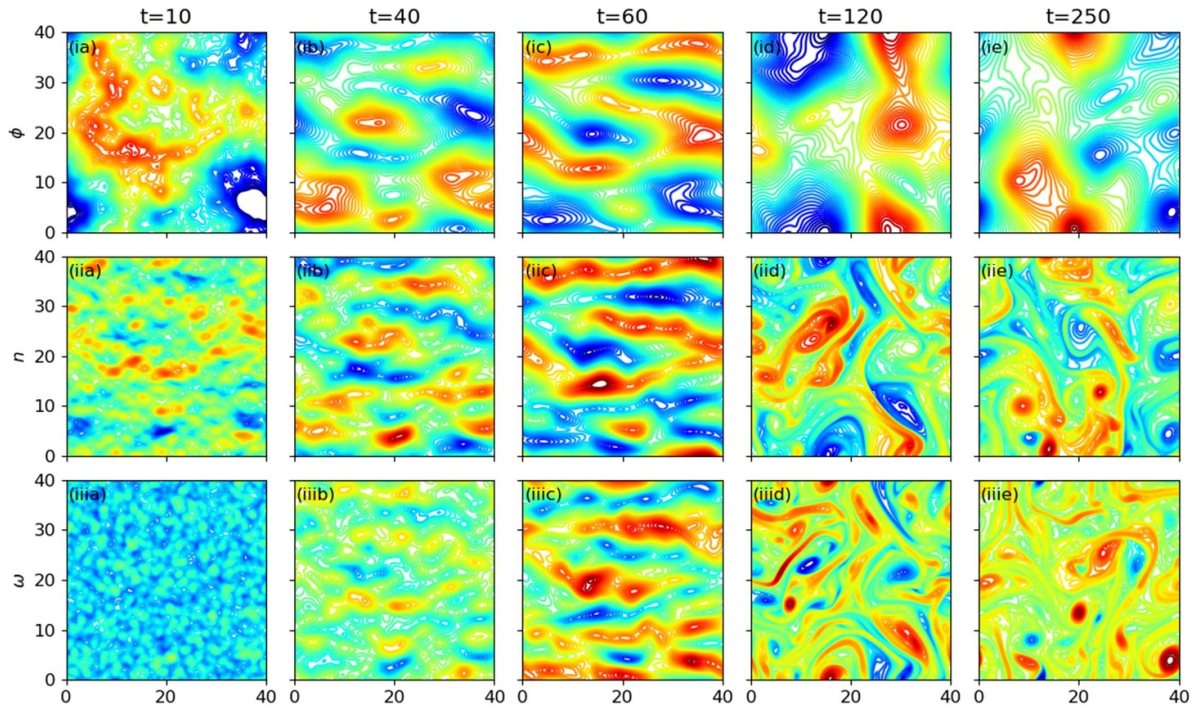

Figure 1. Snapshots of potential (ia)–(ie), density (iia)–(iie) and vorticity (iiia)–(iiie) at selected times t for adiabatic parameter $A = 0.01$.

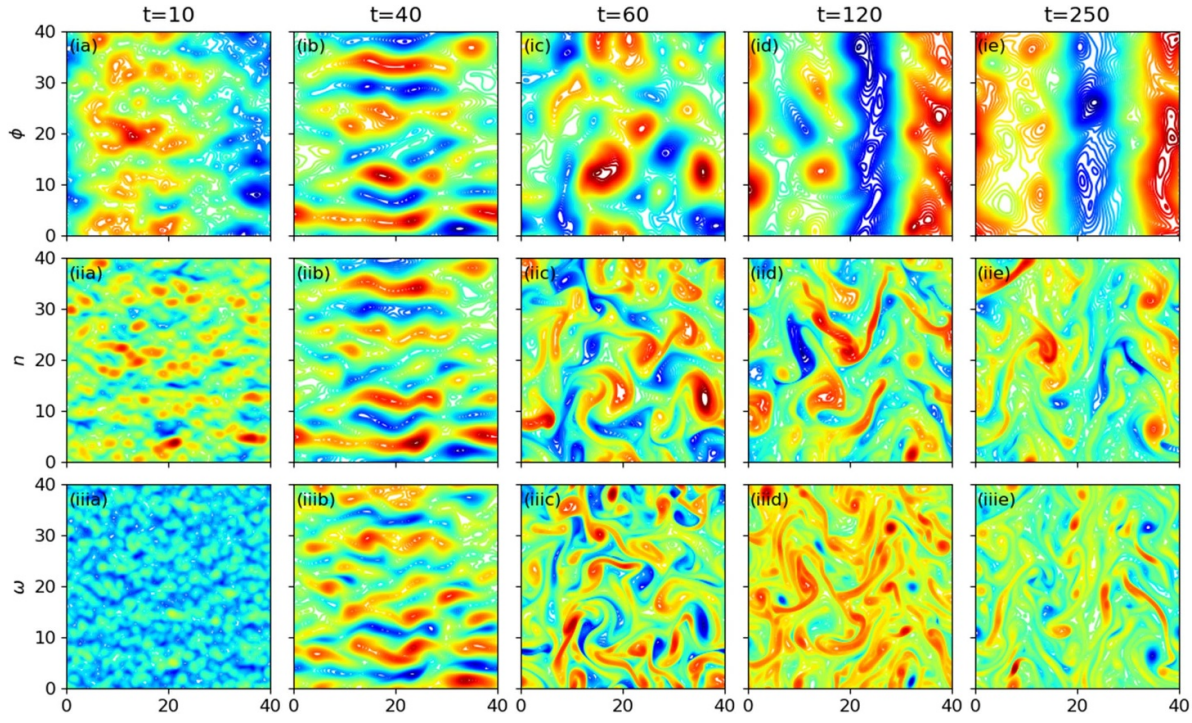

Figure 2. Same as figure 1 for adiabatic parameter $A = 0.1$.

by zonal structures, but this is much less pronounced in the density and in the vorticity fluctuations. In the later stages, large shear develops in the regions between vortices in the turbulent phase and on the boundaries of zonal jets at later times. These regions of intense vorticity have finer spatial structure in comparison with potential and density. It is known that the density has a much weaker zonal component compared with the potential [32], and this is clearly visible in the snapshots at later times in the simulation.

Zonal profiles of the potential, density and vorticity are shown in figures 4–6. The black line in each panel shows zonal component of the $E \times B$ velocity. We find zonal density

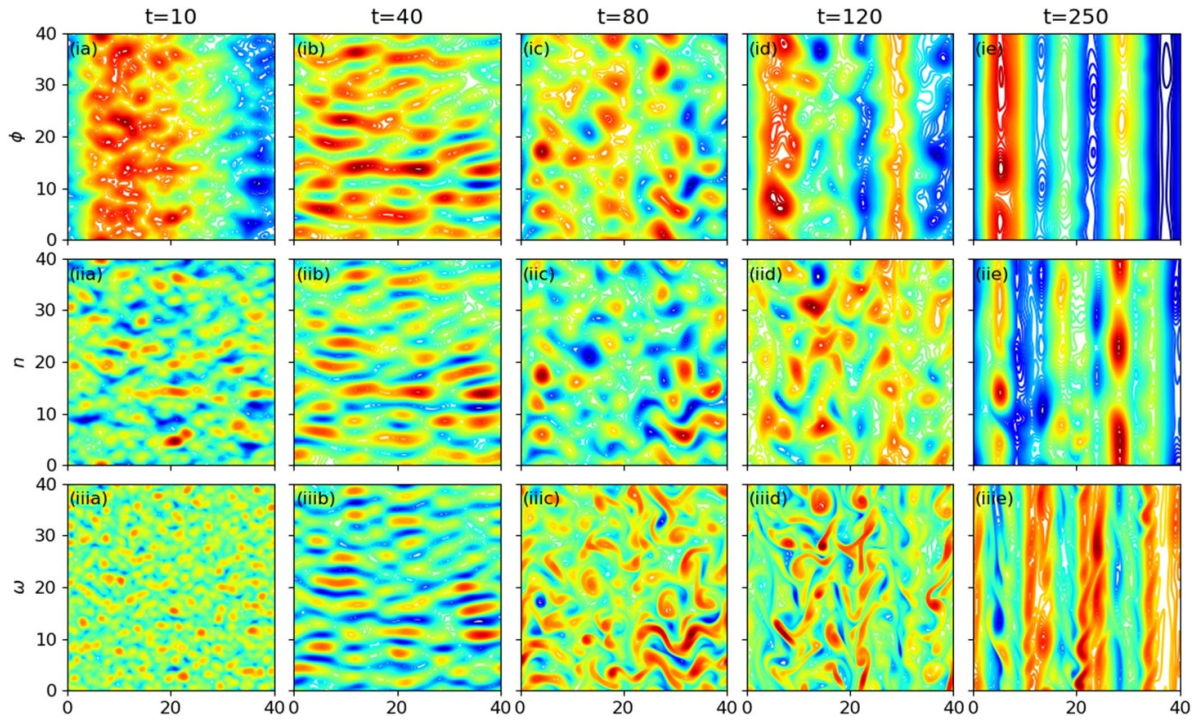

Figure 3. Same as figure 1 for adiabatic parameter $A = 1.0$.

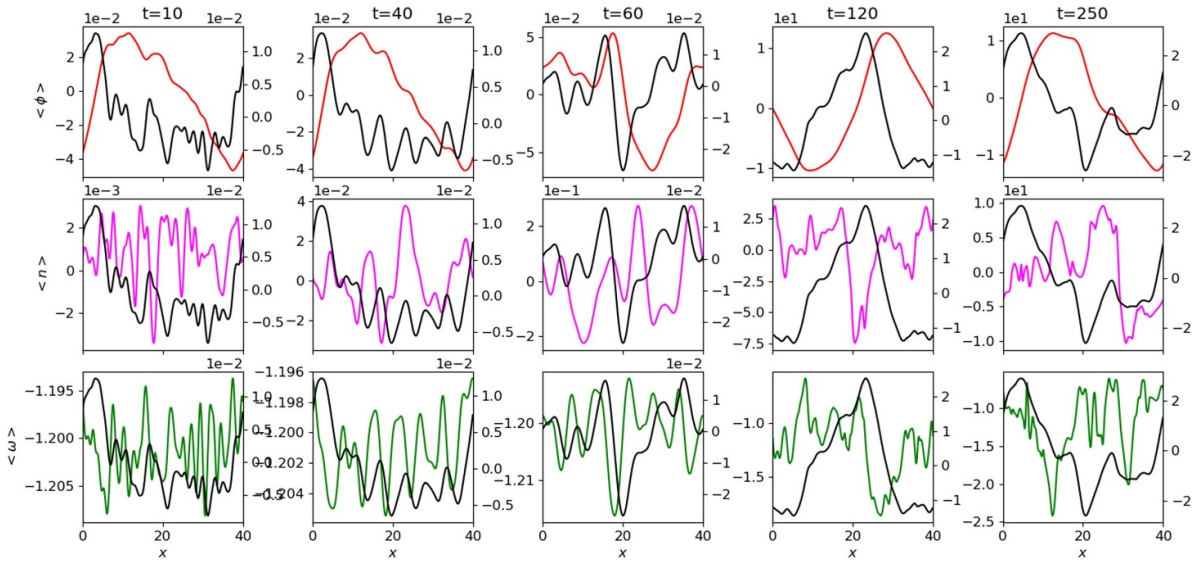

Figure 4. Snapshots of zonal potential (ia)–(ie), zonal density (iia)–(iie) and zonal vorticity (iiia)–(iiie) at times t for adiabatic parameter $A = 0.01$. The black line shows zonal component of the $E \times B$ velocity.

and vorticity patterns often referred to as an $E \times B$ staircase [41–43] in the late stages of the evolution for all values of the parameter A. These are clearest in the final time of zonal density for $A = 0.01$ and in the final zonal vorticity state for $A = 1.0$. Zonal density and vorticity show smaller spatial-scale structures superimposed on the large-scale variation for $A = 0.01$ and $A = 0.1$. These small-scale features are nearly absent for $A = 1.0$. Both density and vorticity patterns are not in phase with zonal potential profile or zonal velocity in all cases.

3.2. *Time-dependent PDF*

In order to gain better understanding of the information rate given by equation (7), it is helpful to examine snapshots of the PDF at various times. PDF of fluctuating parts are calculated at any time-step by sampling the data over the (x, y) domain (that is, over 1024^2 data points) and by constructing histograms. For zonal parts the averaging over y-direction reduces the number of data points to 1024. Therefore, to reduce the

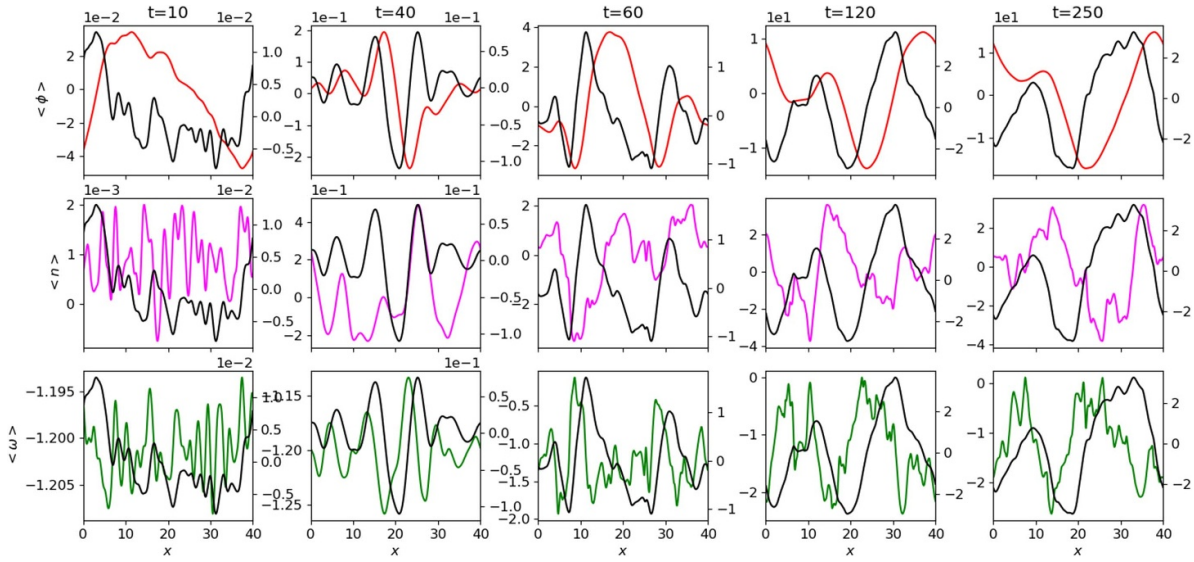

Figure 5. Same as figure 4 for adiabatic parameter $A = 0.1$.

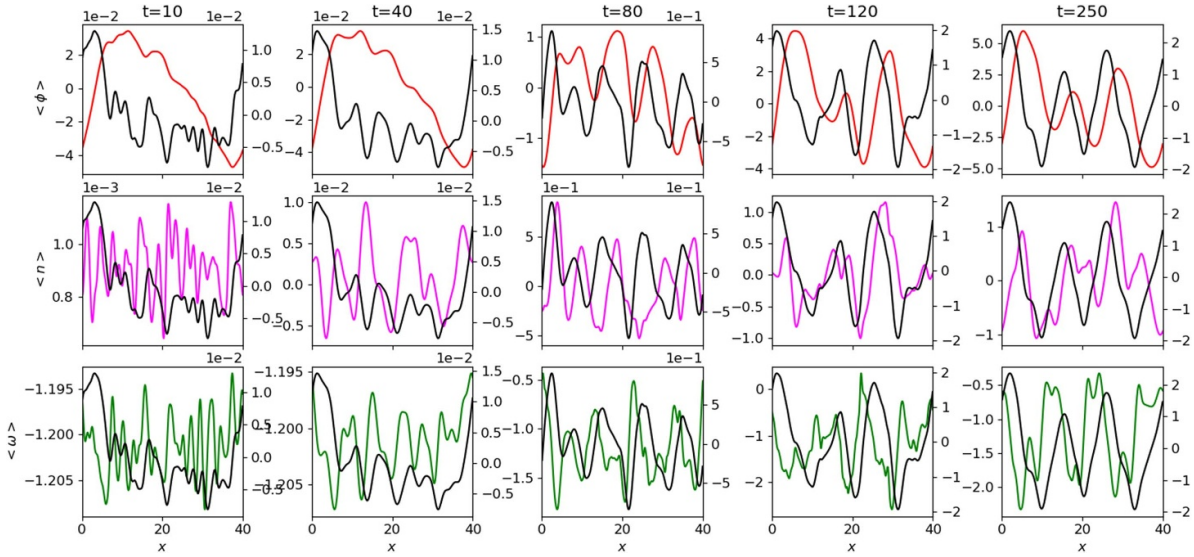

Figure 6. Same as figure 4 for adiabatic parameter $A = 1.0$.

noise in a PDF, we also sample the data over a time window of 100 simulation time-steps, increasing the number of data points 100-fold (with the total 102,400 points). This is justified since taking the characteristic size of the turbulent vortex to be around $10\rho_s$, this time window is of order of a few eddy turnover times $l_0/\tilde{v}$. Here, $\tilde{v}$ is the typical turbulent velocity on the scale l_0. This accumulated PDF is then associated with the time $t + 100\mathrm{d}t$. We note that the construction of a histogram is sensitive to the number of bins used in the process. We applied the Rice University rule [44] which suggests the optimal number of bins for a dataset of n points to be $2\sqrt[3]{n}$.

These PDF are shown in figures 7–9 for the fluctuating component of the three fields, and in figures 10–12, where we present the equivalent PDF for their zonal components. In both figures, the error of the PDF estimate has been calculated assuming the normal distribution of samples in each bin. These errors are small but we have included them in these figures for completeness. There are some notable differences in the PDF of fluctuations in figures 7–9. In the limit of small A, the electrostatic potential fluctuations and the density fluctuations decouple, which is clear from their respective PDF at all times in figure 7. The PDF of all three variables depart from the normal distribution at later times. As the adiabatic parameter A increases, the fluctuations PDF of $\tilde{n}$ and $\tilde{\phi}$ become more similar and for $A = 1.0$ they show nearly identical features. The fluctuating potential PDFs for $A = 1.0$ are nearly Gaussian but have non-zero skewness of alternating sign at later times. A Gaussian distribution with the mean and variance from the fluctuating variable at a given time is shown by a dashed black line in each panel. The PDF of vorticity fluctuations $\tilde{\omega}$ are

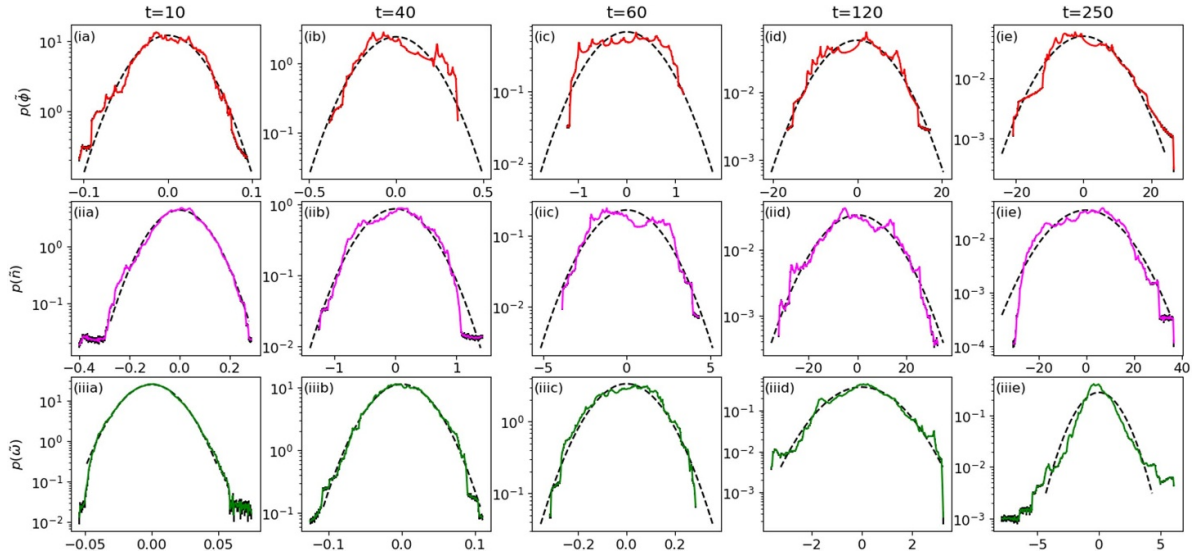

Figure 7. PDFs of fluctuating potential (ia)–(ie), fluctuating density (iia)–(iie) and fluctuating vorticity (iiia)–(iiie) at times t for adiabatic parameter $A = 0.01$. Error bars are shown in black. A Gaussian distribution with the mean and variance from the fluctuating variable at that time is shown by a dashed black line.

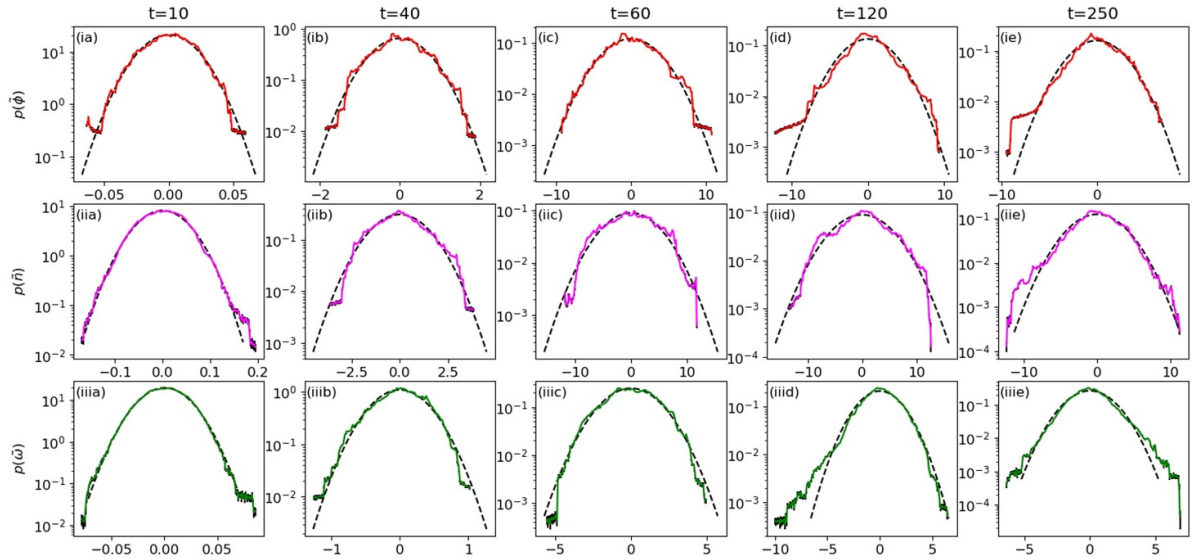

Figure 8. Same as figure 7 for adiabatic parameter $A = 0.1$.

similar to those for $\tilde{n}$ and $\tilde{\phi}$ at the early stages of the system's evolution. Once ZF become significant, at $t = 120$ and at later times, the PDF of vorticity fluctuations are non-Gaussian and resemble those found in hydrodynamic turbulence [45] for all values of A.

Zonal component PDF show significant differences between zonal potential $\langle\phi\rangle$, zonal density $\langle n\rangle$ and zonal vorticity $\langle\omega\rangle$ for all values of the parameter A. Here we are mostly interested in the final stages of the zonal structure development and the final state of the system. It is clear from the visual comparison that the PDFs of $\langle\phi\rangle$ and $\langle n\rangle$ are different at all stages of their evolution. As before, we find the zonal density structure to show small-scale features which remain even in the final time. The range of these PDFs also confirms that the zonal density component contributes less to the total density than the zonal potential contributes to the total potential. Zonal vorticity PDF show a nearly uniform distribution of shear in the turbulent phase, and peaks which correspond to the boundaries of the zonal jets at the final time. We note that the sign of initial zonal vorticity is preserved at all times.

Finally, figure 13 compares the PDF of the fluctuating velocities $\tilde{u}_x$ and $\tilde{u}_y$. Both PDFs show similar evolution, from a small variance distribution at early times to much broader PDF at the final time. The final distributions vary with parameter A, the PDF for $\tilde{u}_x$ and $\tilde{u}_y$ being similar for $A = 0.01$ and $A = 0.1$, but varying strongly for $A = 1.0$, where a much narrower PDF of $\tilde{u}_x$ is seen compared with a PDF of $\tilde{u}_y$. This reflects weak and anisotropic PDF of fluctuating velocity perpendicular to ZF $\langle u_y\rangle$ [46, 47]. Note that the y-axis in this figure uses a linear scale, unlike figures 10–12 where a logarithmic y-axis has

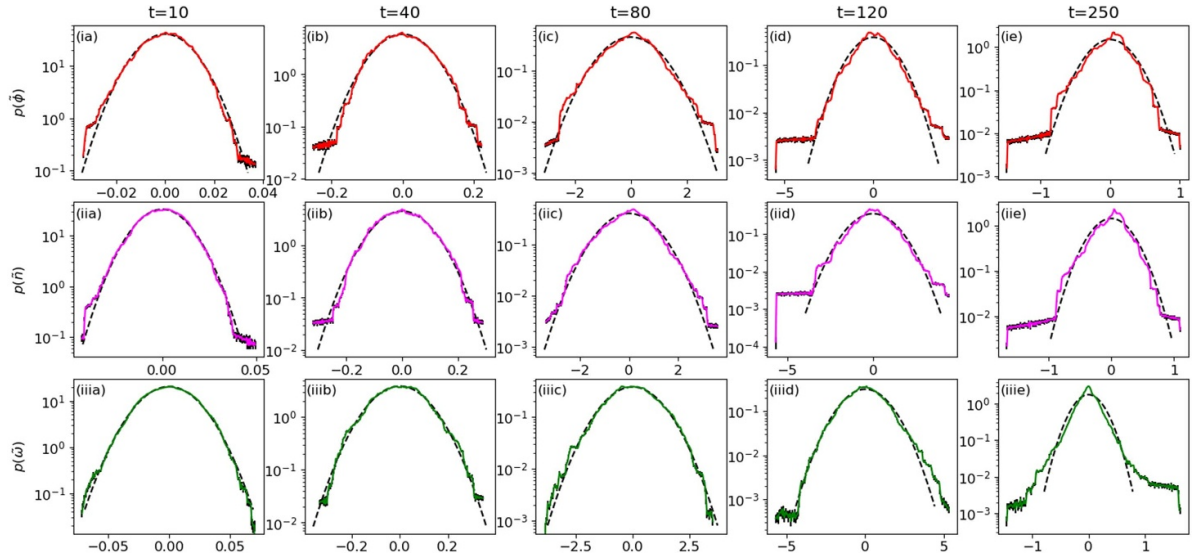

Figure 9. Same as figure 7 for adiabatic parameter $A = 1.0$.

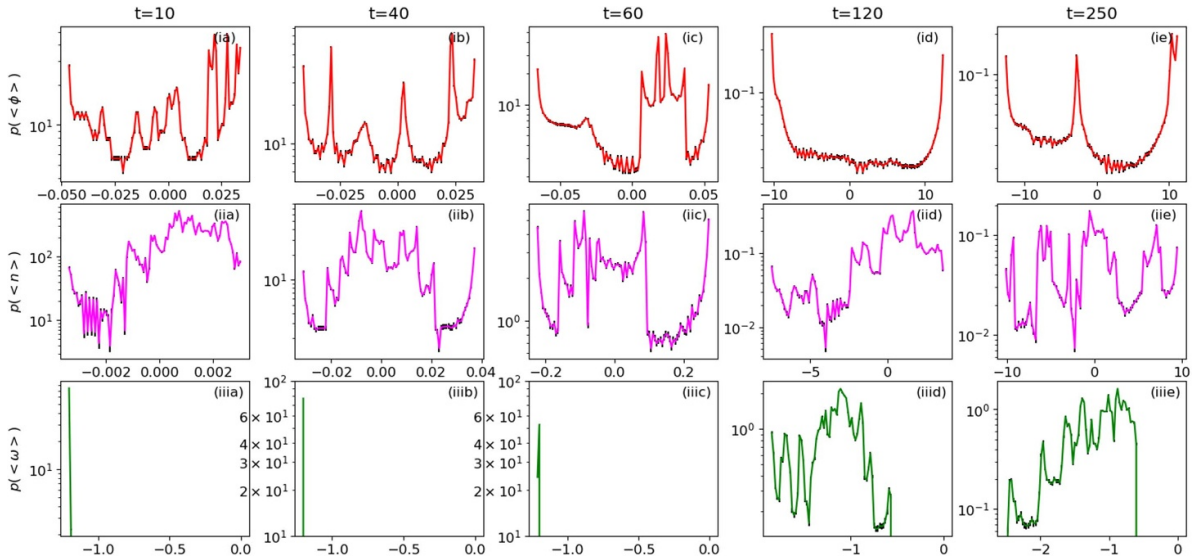

Figure 10. PDFs of zonal potential (ia)–(ie), zonal density (iia)–(iie) and zonal vorticity (iiia)–(iiie) at times t for adiabatic parameter $A = 0.01$. Error bars are shown in black.

been used to emphasise the departure of the vorticity PDFs from the normal distribution at later times.

3.3. Information rate

A visual inspection of the instantaneous PDFs allows only a qualitative appreciation of the evolution of the quantities of interest based on a few temporal snapshots. Information rate Γ provides more complete and quantitative comparison between different fields. For example, similar values of information rate for two different fields is a strong indicator of their direct coupling. Figure 14 shows information rates for all three fields, including their fluctuating and zonal components and for all three values of the parameter A. Panels (ia)–(iiia) of figure 14 show the evolution of the electrostatic potential for all times and for $A = 0.01$, $A = 0.1$ and $A = 1$, respectively. The combined behaviour of its fluctuating and zonal trace gives a quantitative history across all stages of the system evolution for all three different simulations. We note a clear large time-scale variation of zonal component $\langle\phi\rangle$ for all values of A at transition times from drift waves to turbulence, $t \approx 10 - 60$. This large increase in information rate is indicative of the fast energy transfer from fluctuations to zonal component via Reynolds stress. After this initial increase which is common to all three cases, the information rate $\Gamma(\langle\phi\rangle)$ shows different behavior for different values of A. We observe large fluctuations around an approximately constant value $\Gamma(\langle\phi\rangle) \approx 2$ for $A = 0.01$ and at $\Gamma(\langle\phi\rangle) \approx 1$ for $A = 0.1$. For $A = 1.0$ zonal component slowly decreases to reach the value of $\Gamma(\langle\phi\rangle) \approx 0.3$. We find that $\Gamma(\tilde{\phi})$ fluctuates with large variance around a constant value $\Gamma(\tilde{\phi}) \approx 0.5$ at all times for $A = 0.01$ but a secular growth of the information rate can be identified between $t \approx 10 - 60$

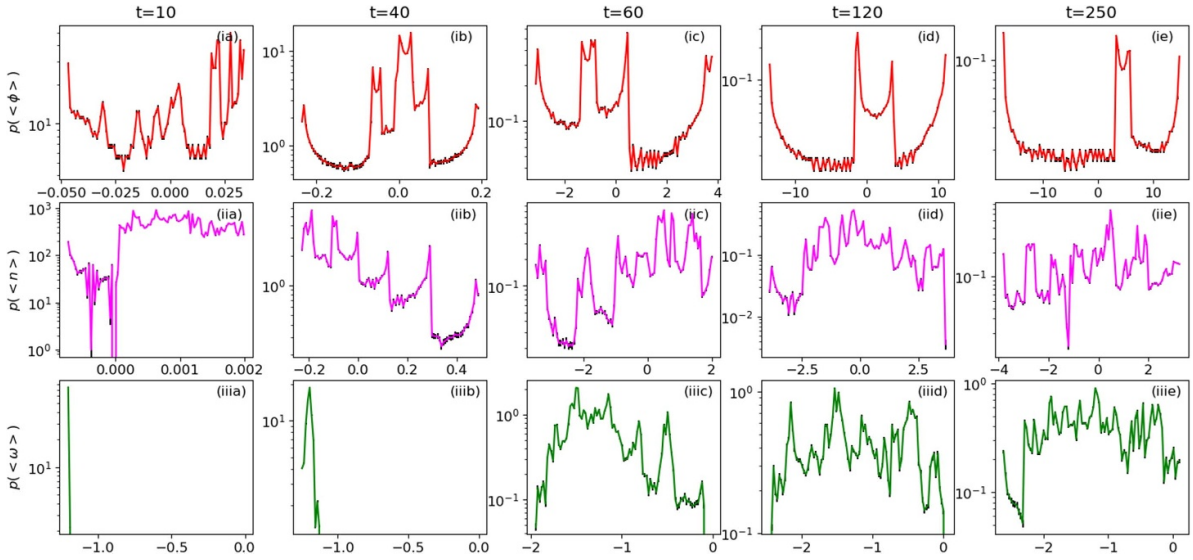

Figure 11. Same as figure 10 for adiabatic parameter $A = 0.1$.

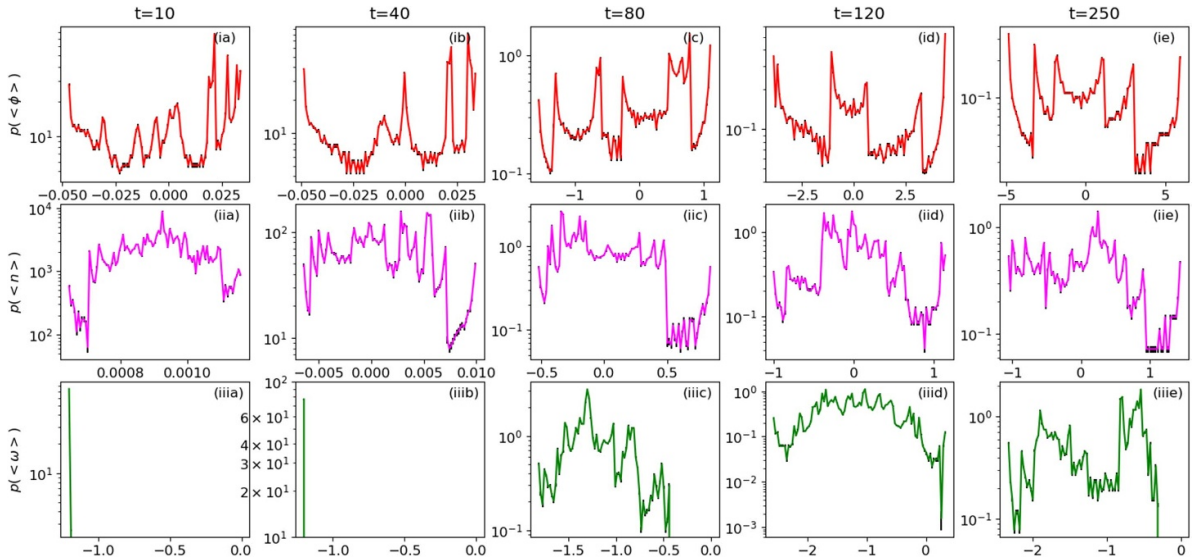

Figure 12. Same as figure 10 for adiabatic parameter $A = 1.0$.

for $A = 0.1$ and $A = 1.0$. For $A = 1.0$, the $\Gamma(\tilde{\phi})$ nearly doubles, from ~ 0.2 to ~ 0.4, during the initial development of turbulent fluctuations. At $t \approx 50$, when Reynolds stress momentum transfer to the zonal component starts, the information rate $\Gamma(\tilde{\phi})$ decreases and then remains nearly constant.

We now contrast the information rate variation of the potential with that found for the fluctuating and zonal densities, shown in the middle column of figure 14. The information rate trace $\Gamma(\tilde{n})$ evolves nearly identically to $\Gamma(\tilde{\phi})$ and the values of the information rates are comparable for all values of A. This is consistent with the past observation that the ratio of fluctuating velocity energy and the internal energy of density fluctuations stay at a fixed ratio during the evolution of the MHW system [32]. Note that similar results are also found for other fluctuating variables, e.g. $\Gamma(\tilde{u}_x), \Gamma(\tilde{u}_y)$, etc (results not shown), corroborating a strong correlation among fluctuating variables.

However, the behaviour of $\Gamma(\langle n \rangle)$ is different from that of $\Gamma(\langle \phi \rangle)$ in all three simulations. After the initial decrease between times $t \approx 0 - 10$, the information rate for zonal density remains nearly constant at $\Gamma(\langle n \rangle) \approx 2 - 3$ between $t \approx 10 - 60$, when $\Gamma(\langle \phi \rangle)$ undergoes its largest increase. For times $t > 60$, $\Gamma(\langle n \rangle)$ increases slightly to about 4 and remains at this value at all times for $A = 0.01$. Similarly, $\Gamma(\langle n \rangle) \approx 4$ at all times $t > 60$ for $A = 0.1$. For $A = 1.0$, the information rate for zonal density decreases to about 0.3 between times $t \approx 120 - 250$. The decreases in the information rate of the zonal density towards values similar to the information rate of the fluctuating density reflects the similar distribution of these fluctuations, showing that the system is now dominated by zonal structures. Note that this is not so for $A = 0.01$, for example, where small scale more isotropic turbulent structures are still present at the latest time. This large difference between

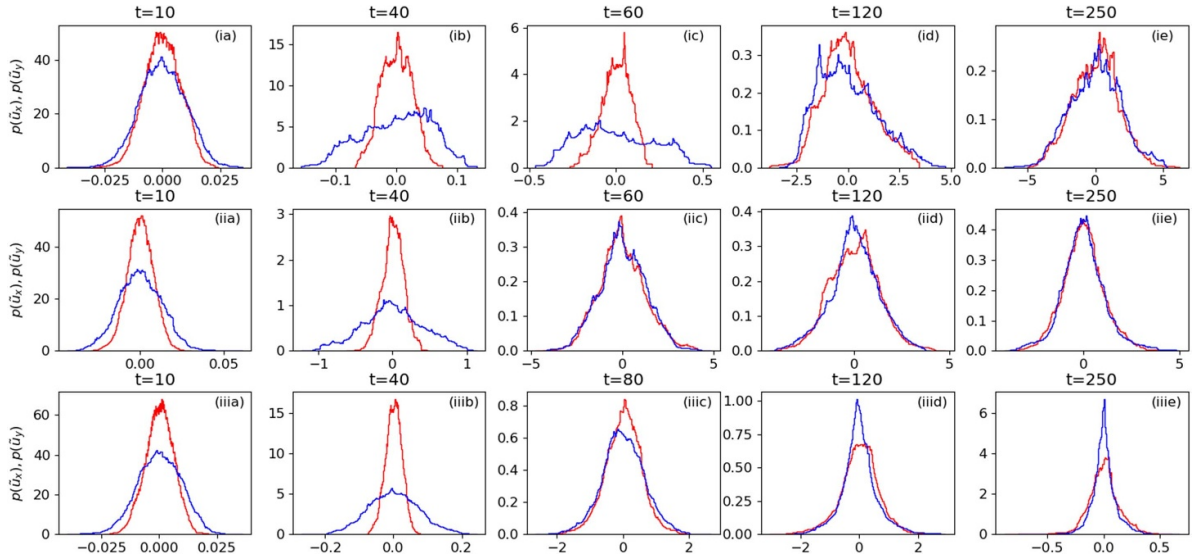

Figure 13. PDFs of $\tilde{u_x}$ (blue) and $\tilde{u_y}$ (red) at times t for adiabatic parameter $A = 0.01$ in panels (ia)–(ie), for $A = 0.1$ in panels (iia)–(iie) and $A = 1.0$ in panels (iiia)–(iiie).

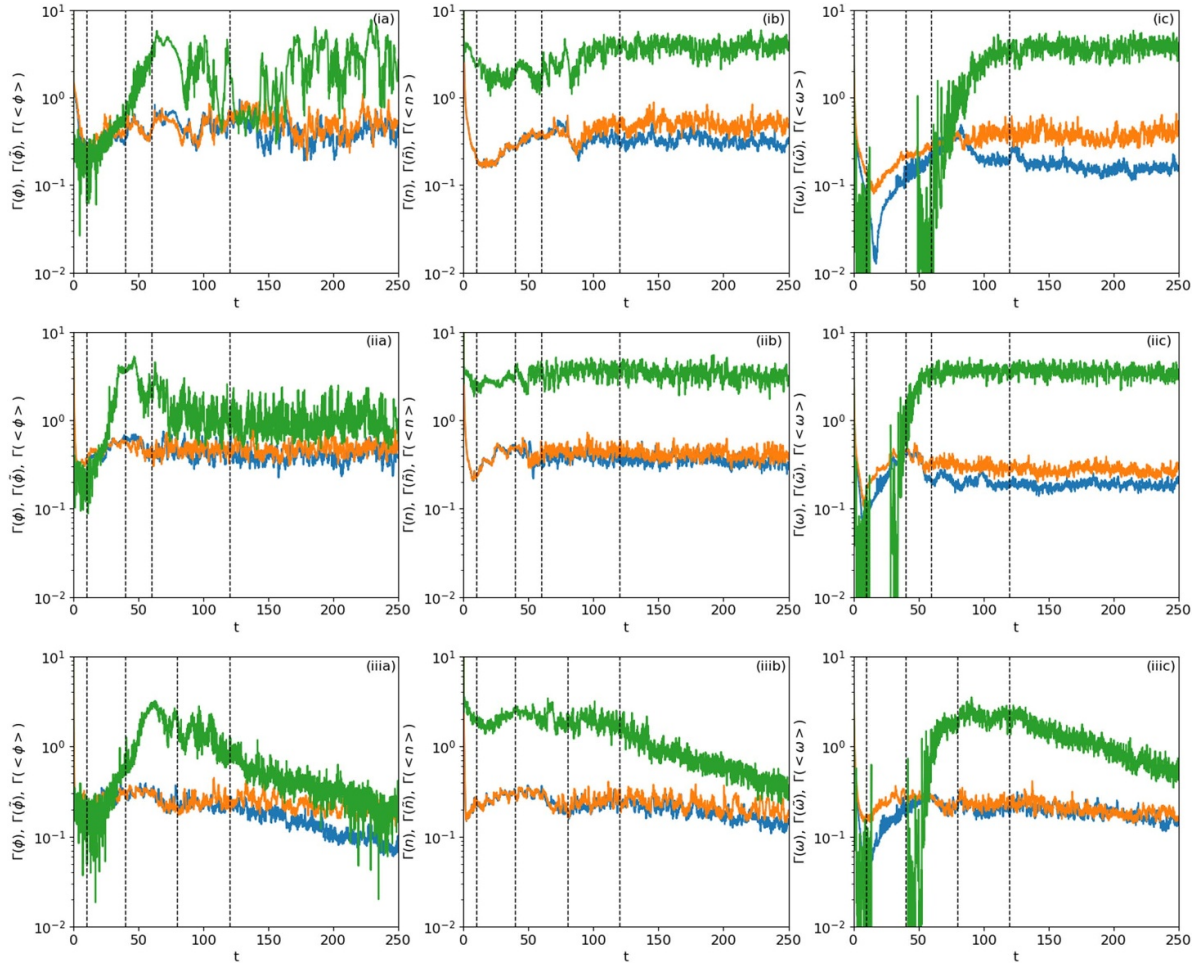

Figure 14. Information rates of potential (ia)–(iiia), density (ib)–(iiib) and vorticity (ic)–(iiic) for $A = 0.01$ in panels (ia)–(ic), $A = 0.1$ in panels (iia)–(iic) and $A = 1.0$ in panels (iiia)–(iiic). Total fields $\Gamma(\phi)$, $\Gamma(n)$ and $\Gamma(\omega)$ are shown in blue, fluctuating components $\Gamma(\tilde{\phi})$, $\Gamma(\tilde{n})$ and $\Gamma(\tilde{\omega})$ are shown in orange and zonal components $\Gamma(\langle\phi\rangle)$, $\Gamma(\langle n\rangle)$ and $\Gamma(\langle\omega\rangle)$ are shown in green. Dashed vertical lines show the times which are the snapshots of the profiles and PDFs.

the evolution of $\Gamma(\langle n\rangle)$ and $\Gamma(\langle\phi\rangle)$ for $t\approx 10-60$ indicates that the zonal density structure may emerge independently of the ZF.

Figures 14(ic)–(iiic) shows the information rates of vorticity. The information rate of fluctuating vorticity $\Gamma(\tilde{\omega})$ follows the same evolution with approximately the same values as $\Gamma(\tilde{\phi})$ and $\Gamma(\tilde{n})$ for all values of A. The information rate of zonal vorticity has negligible values until time $t\approx 50$, after which there is a rapid increase to $\Gamma(\langle\omega\rangle)\approx 2-4$. Conservation of zonal potential entropy $\langle\Pi\rangle$ enforces a strong correlation between time variation of zonal density and zonal vorticity, and this is visible in figure 14, especially in the late stages of the system evolution.

4. Discussion and conclusions

We have applied the concept of information rate to study the evolution of turbulent and zonal components of density, potential and vorticity in the numerical simulation of the MHW Equations. We have varied the adiabatic parameter A to explore three different regimes of the MHW model: from isotropic turbulence dominated regime for $A=0.01$, through the intermediate state with $A=0.1$ to ZF dominated regime for $A=1.0$.

Information rate quantifies the differences between the PDFs of a stochastic variable during its evolution in time, and hence it is particularly suitable for studying non-equilibrium systems. This extends the usual mean field approach which is based on relations between mean values of the variables. For the system with non-Gaussian PDFs, such as these obtained for zonal components of the variables in MHW system, the time variation of mean values may not be a good proxy of the system's dynamics. Due to its normalisation, information rate of different variables can be directly compared, allowing us to draw conclusions about coupling between different fields of the MHW model.

We observe similar values of the information rate for turbulent fluctuations in electrostatic potential, density and vorticity. Thus, the time scale on which the PDF of turbulent fluctuations vary is comparable for all three quantities, reflecting the strong coupling between these quantities during their evolution.

The information rate provides a characteristic time-scale on which the PDF changes significantly. This provides a valuable characteristic of the system's dynamics. We can clearly identify such time-scales in this work, and these are most clearly visible in the zonal components of the relevant variables. One such time-scale is that of transition from drift waves to isotropic turbulence, as seen in the evolution of zonal potential and zonal vorticity at times $t\approx 10-60$ for all values of the parameter A. At these times the information rate of zonal potential is increasing and the information rate of zonal vorticity decreases (it is close to 0 and not visible on the y-axis range of figure 14). This is likely due to a different mechanism of the energy transfer between nonlinearly interacting fluctuations in zonal kinetic energy and zonal enstrophy at the early stages of the simulation. This is supported by zonal profile figures 4–6, where zonal potential has large spatial-scale features and then undergoes a break-up process, while the initial state of zonal vorticity shows small spatial features which later coalesce. Statistically, these different evolution paths are equivalent to a rapid temporal change in PDF of zonal potential (being further from equilibrium) and less temporal change in PDFs of zonal vorticity as it self-organises into larger spatial structures (closer to equilibrium/stationary state). We note that both zonal density and zonal vorticity show much faster time response during their evolution consistent with other studies [43].

The final values of the information rate for zonal component of the electrostatic potential are also informative. Figure 14(ia)–(iiia) gives $\Gamma(\langle\phi\rangle)=\sim 2$, ~ 1 and ~ 0.3 for $A=0.01$, $A=0.1$ and $A=1.0$, respectively. Since $\Gamma(\langle\phi\rangle)\sim\tau_c^{-1}$, this gives the characteristic time for the change in the PDF of $\langle\phi\rangle$ to be $\tau_c\sim 0.5$, $\tau_c\sim 1$ and $\tau_c\sim 3.3$. That is, the time needed for the PDF to change significantly increases by factor of 6-7 for the system dominated by the ZF ($A=1.0$) as compared with the isotropic turbulence ($A=0.01$). This as expected, since the ZF represents a quasi-stationary state with a slow time evolution and so the PDF of the zonal potential is not expected to vary quickly. Note that the information rate of ZF has no relation to the amplitude of ZF.

The impact of zonal density structure on turbulence and the momentum transfer from turbulence to ZF is of particular interest. We find that both density and vorticity zonal profiles are commonly not in phase with the zonal potential profile, which may indicate that the generation mechanism for the density structuring is independent, consistent with previous studies [41, 42]. Particle transport, which drives the time-varying zonal density in (5), depends on the relative phase between density and the radial velocity fluctuations [28]. It has been suggested that the radial modulation of this relative phase due to ZF results in the development of the zonal density pattern [42], forming a corrugated staircase-like structure, such as this found in the final time of zonal density for $A=0.01$ and in the final zonal vorticity state for $A=1.0$.

Data availability statement

The data cannot be made publicly available upon publication because they are not available in a format that is sufficiently accessible or reusable by other researchers. The data that support the findings of this study are available upon reasonable request from the authors.

Acknowledgments

This research is supported by Brain Pool Program funded by the Ministry of Science and ICT through the National Research Foundation of Korea (RS-2023-00284119) and the UK Engineering and Physical Sciences Research Council (EP/W036770/1). EK thanks Seoul National University for support and hospitality.

ORCID iDs

B Hnat https://orcid.org/0000-0001-6498-2953
P Fuller https://orcid.org/0009-0004-2816-619X
E Kim https://orcid.org/0000-0001-5607-6635
R Hollerbach https://orcid.org/0000-0001-8639-0967

References

[1] Wagner F 2018 The history of research into improved confinement regimes *Eur. Phys. J.* H **43** 523–49
[2] Schneider M, Lerche E, Van Eester D, Hoenen O, Jonsson T, Mitterauer V, Pinches S D, Polevoi A R, Poli E and Reich M 2021 Simulation of heating and current drive sources for scenarios of the ITER research plan *Nucl. Fusion* **61** 126058
[3] Lennholm M *et al* 2024 Plasma control for the STEP prototype power plant *Nucl. Fusion* **64** 096036
[4] Ryter F, Orte L B, Kurzan B, McDermott R M, Tardini G, Viezzer E, Bernert M and Fischer R 2014 Fischer R and ASDEX Upgrade Team 2014 Experimental evidence for the key role of the ion heat channel in the physics of the L-H transition *Nucl. Fusion* **54** 083003
[5] Solano E R *et al* 2022 Recent progress in L-H transition studies at JET: tritium, helium, hydrogen and deuterium *Nucl. Fusion* **62** 076026
[6] Biglari H, Diamond P H and Terry P W 1990 Influence of sheared poloidal rotation on edge turbulence *Phys. Fluids* B **2** 1–4
[7] Shaing K C, Crume E C and Houlberg W A 1990 Bifurcation of poloidal rotation and suppression of turbulent fluctuations: a model for the L-H transition in tokamaks *Phys. Fluids* B **2** 1492–8
[8] Itoh S I and Itoh K 1990 Change of transport at L- and H-mode transition *J. Phys. Soc. Japan* **59** 3815–8
[9] Lin Z, Hahm T S, Lee W W, Tang W M and White R B 1998 Turbulent transport reduction by zonal flows: massively parallel simulations *Science* **281** 1835–7
[10] Terry P W, Newman D E and Ware A S 2001 Suppression of transport cross phase by strongly sheared flow *Phys. Rev. Lett.* **87** 185001
[11] Rogers B N, Dorland W and Kotschenreuther M 2000 Generation and stability of zonal flows in ion-temperature-gradient mode turbulence *Phys. Rev. Lett.* **85** 5336
[12] Moyer R A, Tynan G R, Holland C and Burin M J 2001 Increased nonlinear coupling between turbulence and low-frequency fluctuations at the L-H transition *Phys. Rev. Lett.* **87** 135001
[13] Tynan G R, Moyer R A, Burin M J and Holland C 2001 On the nonlinear turbulent dynamics of shear-flow decorrelation and zonal flow generation *Phys. Plasmas* **8** 2691–9
[14] Diamond P H and Kim Y-B 1991 Theory of mean poloidal flow generation by turbulence *Phys. Fluids* B **3** 1626–33
[15] Cziegler I, Tynan G R, Diamond P H, Hubbard A E, Hughes J W, Irby J and Terry J L 2014 Zonal flow production in the L-H transition in Alcator C-Mod *Plasma Phys. Control. Fusion* **56** 075013
[16] Diamond P H, Itoh S-I, Itoh K and Hahm T S 2005 Zonal flows in plasma – a review *Plasma Phys. Control. Fusion* **47** R35
[17] Hnat B, Gadgil S, Kirk A, Militello F, Walkden N and Team M A S T 2018 Experimental constraint on the radial mode number of the geodesic acoustic mode from multi-point Langmuir probe measurements in MAST Ohmic plasma *Plasma Phys. Control. Fusion* **60** 085016
[18] Rosenbluth M N and Hinton F L 1998 Poloidal flow driven by ion-temperature-gradient turbulence in tokamaks *Phys. Rev. Lett.* **80** 724
[19] Kim E and Diamond P H 2003 Zonal flows and transient dynamics of the L-H transition *Phys. Rev. Lett.* **90** 185006
[20] Kim E and Hollerbach R 2020 Time-dependent probability density functions and information geometry in the fusion L-H transition *Phys. Rev. Res.* **2** 023077
[21] Fuller P, Kim E, Hollerbach R and Hnat B 2023 Time-dependent probability density functions, information geometry and entropy production in a stochastic prey-predator model of fusion plasmas *Phys. Plasmas* **30** 102502
[22] Kim E and Thiruthummal A A 2024 Stochastic dynamics of fusion Low-to-High confinement mode (L-H) transition: correlation and causal analyses using information geometry *Entropy* **26** 17
[23] Groebner R J, Burrell K H and Seraydarian R P 1990 Role of edge electric field and poloidal rotation in the L-H transition *Phys. Rev. Lett.* **64** 3015
[24] McKee G R, Fonck R J, Jakubowski M, Burrell K H, Hallatschek K, Moyer R A, Nevins W, Rudakov D L and Xu X 2003 Observation and characterization of radially sheared zonal flows in DIII-D *Plasma Phys. Control. Fusion* **45** A477
[25] Liu A D *et al* 2009 Characterizations of low-frequency zonal flow in the edge plasma of the HL-2A tokamak *Phys. Rev. Lett.* **103** 095002
[26] Hasegawa A, Maclennan C G and Kodama Y 1979 Nonlinear behavior and turbulence spectra of drift waves and Rossby waves *Phys. Fluids* **22** 2122–9
[27] Hasegawa A and Wakatani M 1987 Self-organization of electrostatic turbulence in a cylindrical plasma *Phys. Rev. Lett.* **59** 1581
[28] Dewhurst J M, Hnat B and Dendy R O 2009 The effects of nonuniform magnetic field strength on density flux and test particle transport in drift wave turbulence *Phys. Plasmas* **16** 072306
[29] Numata R, Ball R and Dewar R L 2007 Bifurcation in electrostatic resistive drift wave turbulence *Phys. Plasmas* **14** 102312
[30] Del Sarto D and Ghizzo A 2017 Hasegawa-Wakatani and modified Hasegawa-Wakatani turbulence induced by ion-temperature-gradient instabilities *Fluids* **2** 65
[31] Gallagher S, Hnat B, Connaughton C, Nazarenko S and Rowlands G 2012 The modulational instability in the extended Hasegawa-Mima equation with a finite Larmor radius *Phys. Plasmas* **19** 122115
[32] Stoltzfus-Dueck T 2016 Parallel electron force balance and the L-H transition *Phys. Plasmas* **23** 054505
[33] Kim E 2021 Information geometry, fluctuations, non-equilibrium thermodynamics and geodesics in complex systems *Entropy* **23** 1393
[34] Kim E 2018 Investigating information geometry in classical and quantum systems through information length *Entropy* **20** 574
[35] Hasegawa A and Wakatani M 1983 Plasma edge turbulence *Phys. Rev. Lett.* **50** 682
[36] Hasegawa A and Mima K 1978 Pseudo-three-dimensional turbulence in magnetized nonuniform plasma *Phys. Fluids* **21** 87–92
[37] Guel-Cortez A-J and Kim E 2021 Information geometric theory in the prediction of abrupt changes in system dynamics *Entropy* **23** 694
[38] Farre-Kaga H J, Andrew Y, Dunsmore J, Kim E, Rhodes T L, Schmitz L and Yan Z 2023 Time-dependent probability density function analysis of H-mode transitions *Europhys. Lett.* **142** 64001

[39] Anderson J, Kim E, Hnat B and Rafiq T 2020 Elucidating plasma dynamics in Hasegawa-Wakatani turbulence by information geometry *Phys. Plasmas* **27** 022307
[40] Kim E, Heseltine J and Liu H-L 2020 Information length as a useful index to understand variability in the global circulation *Mathematics* **8** 299
[41] Dif-Pradalier G *et al* 2015 Finding the elusive $E \times B$ staircase in magnetized plasmas *Phys. Rev. Lett.* **114** 085004
[42] Leconte M and Kobayashi T 2021 Zonal profile corrugations and staircase formation: role of the transport crossphase *Phys. Plasmas* **28** 014503
[43] Zhang Y and Krasheninnikov S I 2020 Influence of zonal flow and density on resistive drift wave turbulent transport *Phys. Plasmas* **27** 122303
[44] De La Rubia J M 2024 Rice University rule to determine the number of bins *Open J. Stat.* **14** 119–49
[45] Frisch U 1995 *Turbulence: The Legacy of A.N. Kolmogorov* (Cambridge University Press)
[46] Burrell K 1997 Effects of velocity shear and magnetic shear on turbulence and transport in magnetic confinement devices *Phys. Plasmas* **4** 1499
[47] Kim E 2006 Consistent theory of turbulent transport in two dimensional magnetohydrodynamics *Phys. Rev. Lett.* **96** 084504